Ethanol Steam Reforming on Rh Catalysts: Theoretical and Experimental Understanding

6 AUTHORS, INCLUDING:

Jia Zhang
Institute Of High Performance Computing
18 PUBLICATIONS   **345** CITATIONS

SEE PROFILE

Ziyi Zhong
Institute of Chemical and Engineering Sciences
184 PUBLICATIONS   **5,182** CITATIONS

SEE PROFILE

Xiaoming Cao
East China University of Science and Techno…
22 PUBLICATIONS   **341** CITATIONS

SEE PROFILE

Luwei Chen
Institute of Chemical and Engineering Sciences
46 PUBLICATIONS   **1,752** CITATIONS

SEE PROFILE

Ethanol Steam Reforming on Rh Catalysts: Theoretical and Experimental Understanding

Jia Zhang,*,[†] Ziyi Zhong,[‡] X.-M. Cao,[§] P. Hu,[§,⊥] Michael B. Sullivan,[†] and Luwei Chen[‡]

[†]Institute of High Performance Computing, Agency for Science, Technology and Research, Singapore, 1 Fusionopolis Way #16-16 Connexis, Singapore 138632

[‡]Institute of Chemical Engineering and Sciences, Agency for Science, Technology and Research, Singapore, 1 Pesek Road, Jurong Island, Singapore 627833

[§]State Key Laboratory of Chemical Engineering, Centre for Computational Chemistry and Research Institute of Industrial Catalysis, East China University of Science and Technology, Shanghai 200237, People's Republic of China

[⊥]School of Chemistry and Chemical Engineering, Queen's University of Belfast, Belfast, BT9 5AG, United Kingdom

S *Supporting Information*

ABSTRACT: Through combined theoretical and experimental efforts, the reaction mechanism of ethanol steam reforming on Rh catalysts was studied. The results suggest that acetaldehyde (CH_3CHO) is an important reaction intermediate in the reaction on nanosized Rh catalyst. Our theoretical work suggests that the H-bond effect significantly modifies the ethanol decomposition pathway. The possible reaction pathway on Rh (211) surface is suggested as $CH_3CH_2OH \rightarrow CH_3CH_2O \rightarrow CH_3CHO \rightarrow CH_3CO \rightarrow CH_3 + CO \rightarrow CH_2 + CO \rightarrow CH + CO \rightarrow C + CO$, followed by the water gas shift reaction to yield H_2 and CO_2. In addition, we found that the water-gas shift reaction, not the ethanol decomposition, is the bottleneck for the overall ethanol steam reforming process. The CO + OH association is considered the key step, with a sizable energy barrier of 1.31 eV. The present work first discusses the

mechanisms and the water effect in ethanol steam reforming reactions on Rh catalyst from both theoretical and experimental standpoints, which may shed light on designing improved catalysts.

KEYWORDS: *ethanol steam reforming, Rh catalyst, reaction mechanism, DFT calculations, real-time GC/MS analysis*
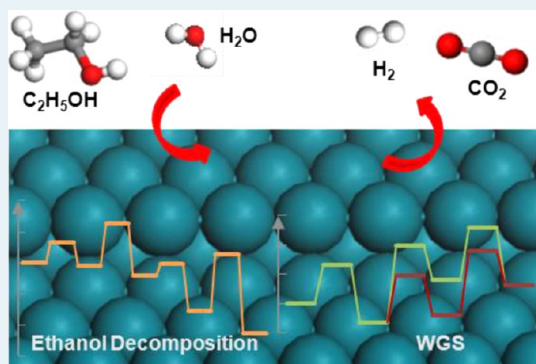
1. INTRODUCTION

In recent years, the rising global energy demands and the growth of the environmental pollution have motivated people to tap alternative fuels and sustainable development. Among all possible alternative fuels, hydrogen is considered as an ideal energy carrier of the future.[1] Apart from commonly used methane[2] and methanol,[3] ethanol conversion to hydrogen has drawn much attention not only because of its nontoxicity and ease of handling, but most importantly, it can be produced from biomass fermentation, which provides a viable way for H_2 production from renewable resources.[4] Currently, H_2 can be generated by three typical routes, including steam reforming (SR), partial oxidation, and oxidative steam reforming (OSR),[5] in which the SR reaction is the widely used thermochemical process[1] because it provides the highest yield of hydrogen, that is, the molar ratio of H_2/CO_2 is 3. In fact, ethanol steam reforming (ESR) has been extensively studied in past years.[6−17] Several research groups have systematically reviewed the recent progress in ethanol steam reforming from catalyst performance to reaction mechanism.[1,4,5] It appears that noble metal catalysts (e.g., Rh, Pt, Ru)[6,8,9] and nonnoble catalyst (Ni, Co),[12−15] as well as bimetallic catalysts such as Ni−Rh,[16] Pt−Co,[14] and

RhPt,[17] are promising candidates for ESR reactions. In addition, the supported oxide could affect the activity and the stability of the catalyst.[16,18] It was reported the neutral support is more effective for ethanol dehydrogenation.[19]

Among the noble metal catalysts, Rh is the best catalyst for ESR reactions because of its good ability to break the C−C bond and the high hydrogen yield.[4,20] Frusteri et al. investigated MgO-supported Rh, Pd, Ni, and Co catalysts in ESR reactions and found that Rh is at least 2.2 times more active than the other three metal catalysts.[21] At present, Rh catalysts used in the ESR process have been well studied using a wide array of experimental approaches: from catalyst preparation to characterization and from deactivation to regeneration, as well as from catalytic performance to mechanism studies.[5,6,22−31] It can be seen that the preparation method,[23] reaction temperature,[7,27] the nature of the oxide support,[29,30] as well as the steam/ethanol molar ratio,[32] affect the final ethanol conversion and hydrogen selectivity. Compared with the efforts in experimental

areas, theoretical research in this area is lagging behind. The current theoretical work has concentrated on the ethanol decomposition on the metal surface.[33−35] Of course, these fundamental studies have provided some clues to understanding ESR, but it is still far away from the actual reforming reaction because some important factors are skipped.

As mentioned, in the ethanol steam reforming process, water is a key reactant; however, to date, only a few theoretical works considered the influence of OH/O species on the catalytic process.[36,37] For example, Ma and co-worker investigated ethanol reforming on a Co(0001) surface using density functional theory and proposed that the dehydrogenation of ethoxy is the rate-determining step.[36] In addition, very recently, Syu and Wang studied the OSR process of ethanol on a Rh(111) surface. The results revealed that both CH_3CHO and CH_2CH_2O are key intermediates and the O-precovered Rh(111) surface does not improve the decomposition step, but helps the oxidation step.[37] However, as yet, the detailed reaction mechanism of ESR on nanosized Rh catalyst is still unclear. Although some experimental results have suggested that acetaldehyde is an important intermediate for ESR,[5,20] previous theoretical calculations on ethanol dissociation have indicated that no acetaldehyde can be observed in the course of direct ethanol decomposition on both Rh(111) and Rh (211) surface.[34,38] The contradiction implies that water plays a vital role in the whole chemical process, and it is possible to thoroughly change the reaction pathway. Thus, in this work, we try to tackle these puzzles from both a theoretical and an experimental point of view. In our experimental work, the Rh nanoparticle is 4−5 nm, where the step is the most common defect and usually active in catalytic reactions.[39,40] Thus, the stepped Rh(211) surface as a prototypical surface was studied in the theoretical work to shed some lights on what happened on the Rh nanosized catalyst.

2. COMPUTATIONAL AND EXPERIMENTAL METHOD

DFT calculations were performed using the Vienna Ab Initio Simulation Package,[41,42] in which a plane-wave basis set is used. The electron−ion interaction was modeled by the projector-augmented wave method.[43,44] The (PW91) form of the generalized-gradient approximation was used for the exchange and correlation functional.[45] The plane-wave cutoff energy was set to 400 eV. The calculated lattice constant of 3.841 Å for Rh bulk is consistent with the experimental and theoretical values.[46,47]

For surface calculations, the $p(2 \times 3)$ Rh(211) surface is simulated using a slab supercell approach with periodic boundary conditions. The slab contained four layers of metal atoms, of which the bottom two layers are fixed and top two metal layers are allowed to move freely. We used a vacuum region of 15 Å, which is large enough to avoid interactions between adsorbates and slab images. A $2 \times 3 \times 1$ k-point mesh with Monkhorst−Pack scheme was used for surface calculations. All transition states (TSs) were located using the constrained minimization technique.[48] For important reactions, the zero-point energy (ZPE) was calculated to correct the reaction barriers (see Supporting Information Table S3).

In this work, we studied the adsorption of H_2O and some ethanol-derived species on Rh(211) surface. The adsorption energy is defined as $E_{ad} = E_{slab+A} - E_{slab} - E_A$, where the E_{slab+A} is the total energy of the slab with adsorbate, E_{slab} is the energy of clean Rh(211) surface, and E_A is the energy of gas-phase adsorbate A. By definition, a negative value corresponds to

exothermic adsorption. In addition, the reaction energy is defined as $\Delta E = E_{product} - E_{reactant}$. Herein, spin-polarized calculations were carried out for gas-phase radical species derived from ethanol.

■ EXPERIMENTAL SECTION

The ZrO_2 support was prepared by a hydrothermal method as described elsewhere[23] and calcined at 680 °C for 5 h in air after drying. One weight percent Rh was deposited onto the ZrO_2 support employing the conventional impregnation method using $RhCl_3$ as the precursor. The supported Rh catalysts were calcined in air at 500 °C for 4 h.

The catalytic evaluation for ESR was performed in a fix-bed microreactor. For each individual catalytic run, 50 mg of catalyst was loaded and reduced in H_2 at 250 °C for 0.5 h prior to the reaction. Following that, a mixture of ethanol and water with a molar ratio of $EtOH/H_2O = 1: 10$ was pumped in at a flow rate of 0.005 mL min^{-1}, vaporized, and carried into the catalyst bed by a N_2 carrier gas flow (the EtOH concentration was 1% in the gas phase). The outlet gas products were analyzed using an online GC/MS system, by which various reactants, intermediates, and products in gas phase were monitored in real time.

3. RESULTS AND DISCUSSION

In our previous experimental work,[23] we have investigated ethanol steam reforming reactions on Rh catalysts supported on ZrO_2-based oxides. It was reported that $v_{C=O}$ vibration (the peak at 1736 cm^{-1}) and v_{CH_3} vibration (the peaks at 2905 and 2979 cm^{-1}) were observed in the DRIFTS study, which indicated that acetyl species can be rapidly formed on the Rh/ZrO_2 catalyst. However, the origin of the acetyl species is not so clear. Recently, the further mechanism studies were performed by employing a GC/MS system to monitor the reaction intermediates in real time, and the results are shown in Figure 1. It can be seen that a C_2H_4O species is formed in the ethanol steam reforming process. In Figure 1, the conversion of ethanol (the red line) always decreases and the C_2H_4O species increases (the orange line) with the change of the reaction
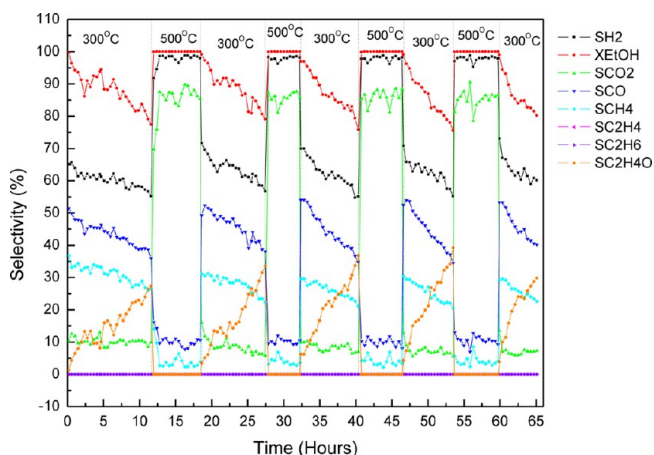

Figure 1. GC/MS real-time measurement of ethanol (EtOH) conversion (X_{EtOH}) and selectivities (S) of various chemical species produced in the course of the ESR reaction when the reaction temperature was jumped between 300 and 500 °C alternately. During the reaction, the selectivities of C_2H_4 and C_2H_6 were always zero (the two bottom lines).
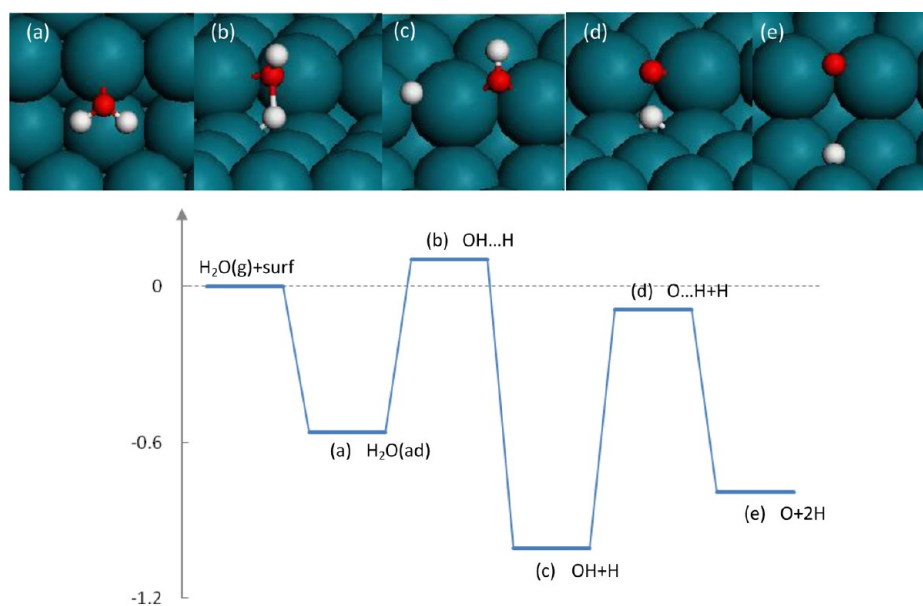
Figure 2. Snapshots and energy profile for H_2O dissociation process.

Table 1. Adsorption Energies and Geometry Parameters of Some Intermediates for Ethanol Decomposition with the Aid of Water on Rh(211) Surface

species	E_{ad} (eV)	$d_{C(\alpha)\text{-Rh}}$ (Å)	$d_{C(\beta)\text{-Rh}}$ (Å)	$d_{O\text{-Rh}}$ (Å)	adsorption site
CH₃CHO	−1.09	2.093		2.057	oxymetallacycle species via C_α and O at Rh step
CH₂CHO	−2.87	2.304	2.164	2.008	oxymetallacycle species via C=O and C_β at Rh step
trans-COOH	−2.91	1.982		2.139	oxymetallacycle species via C and O at Rh step
cis-COOH	−2.95	1.979		2.144	oxymetallacycle species via C and O at Rh step
CH₃OH	−0.58			2.234	e-top via O
CH₂OH	−2.35	2.246		2.054	oxymetallacycle species via C and O at Rh step
CHOH	−3.82	2.038/2.046			e-bri via C
CH₂O	−1.31	2.100		1.988	oxymetallacycle species via C and O at Rh step
CH₃COOH (C=O adsorption mode)	−0.62	2.338		2.206/2.215	e-bri via carbonyl O, off-e top site via carbonyl C
CH₃COOH (O=C−O adsorption mode)	−0.57	2.185		2.124 (carbonyl O)/2.286 (hydroxyl O)	oxymetallacycle species via C=O and hydroxyl O at Rh step
CH₂COOH	−2.32		2.116	2.222	oxymetallacycle species via C_β and hydroxyl O at Rh step
H₂O	−0.56			2.284	e-top via O

temperature from 500 to 300 °C, whereas both of them are completely decomposed at 500 °C. Indeed, there are two possible structural isomers for C_2H_4O species, including acetaldehyde (CH₃CHO) and 1-hydroxyethylidene (CH₃COH); however, the structure cannot be identified from the experimental results. In this study, DFT calculation was performed to qualitatively confirm key reaction intermediates, provide interpretations for experimental observations, and propose possible reaction mechanisms for ESR process.

3.1. Adsorption and Dissociation of H_2O. H_2O is a key reactant in the ethanol steam reforming reaction; thus, in this work, we first studied the adsorption and dissociation behavior of H_2O on a stepped Rh(211) surface. We found that H_2O is molecularly adsorbed on the Rh (211) surface and prefers the off-top site at the step edge. The water molecule (the plane formed by H−O−H) is almost parallel to the (100)-type step, with an O−Rh distance of 2.284 Å and an adsorption energy of −0.56 eV, which is close to the literature value of −0.63 eV (−61 KJ/mol) at the top of the edge on Rh(221) surface.[49] It is

obvious that the water adsorption is stronger at the step edge than that on the flat Rh(111) surface, where the most favorable top site leads to an adsorption energy ranging from −0.35 to −0.42 eV.[49−53] Because we have reported the adsorption behaviors of OH, O and H on Rh (211) in our previous publications (all species prefer the bridge site at the step edge),[38] here, we investigated only the water dissociation process directly.

Figure 2 shows the snapshots of water decomposition on Rh (211). It can be seen that the sequential O−H bond-breaking occurs on the surface step rather than on the step edge. At the TS_{H-OH} (Figure 2b), the [H···OH] complex bridges on the step, where OH is located on an off-edge-bridge site with Rh−O of 2.214 and 2.179 Å, and H is located on the bridge site of the lower (111) terrace with an Rh−H of 2.001 and 2.075 Å. The calculated dissociation barrier of water is 0.66 eV, which is close to that on Rh (111) (63 kJ/mol) and Rh (221) (61 kJ/mol).[49] The further dissociation of the OH group to produce adsorbed O and H has a barrier of 0.92 eV (0.75 eV with ZPE
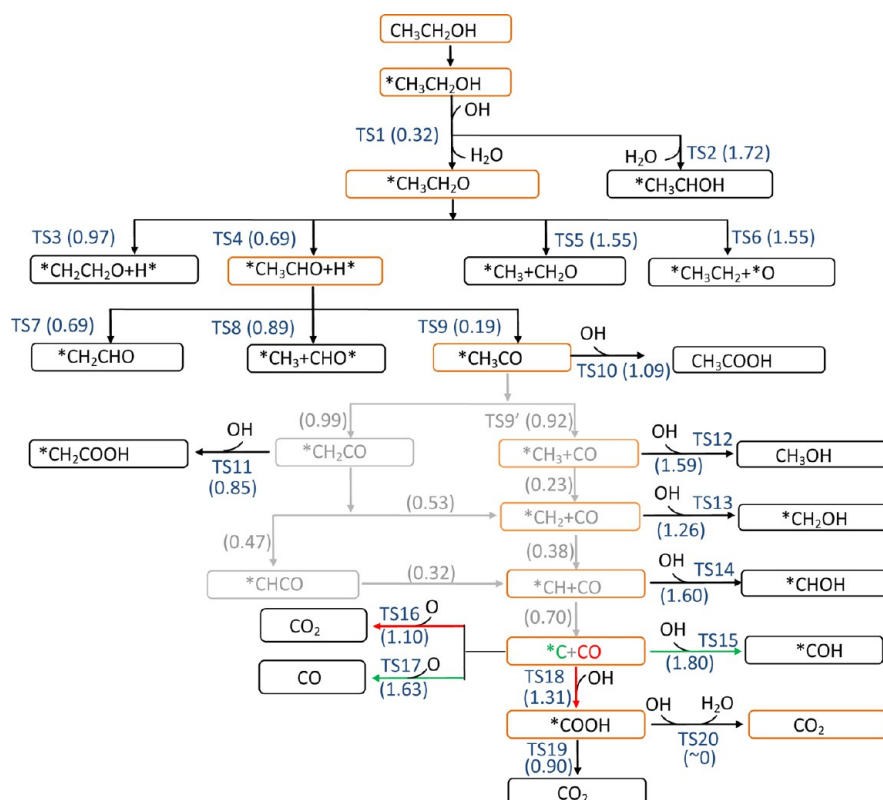
Figure 3. The calculated possible reaction pathways for ethanol decomposition on a Rh(211) surface with the aid of water. Intermediates on the most likely reaction path are in orange boxes. The parenthesized energy barriers are in eV. The gray part has been reported in our previous publication.[38]

correction). At TS_{O-H} (Figure 2c), similarly, the O−H bond is breaking on the step with a O−H distance of 1.489 Å; however, it is longer than the one in TS $_{H-OH}$ (d_{O-H} = 1.392 Å). It is worth noting that the H_2O dissociation is an exothermal process with a reaction energy of 0.45 eV; in contrast, the further dissociation of the OH group is an endothermal reaction. As a consequence, the energy barrier of the O + H association is 0.22 eV lower than that of the O−H dissociation. Although in H_2O, the first H abstraction is easier than the second one, at the actual experimental temperature (300−500 °C), both a hydroxyl group and an oxygen atom could exist on the catalyst surface. In addition, another important elementary step of adsorbed H + H recombination was also studied here. It can be seen that the energy barrier is 0.52 eV (0.56 eV after ZPE correction) for H + H association, which is lower than those required by both H_2O (0.66 eV with or without ZPE correction) and an OH group (0.92 eV/0.75 eV with or without ZPE correction) dissociation process. However, Tang and Liu studied the water gas shift reaction over Cu/ZrO_2 and found that H + H recombination (1.03 eV) has a higher energy barrier compared with the decomposition of water (0.76 eV).[54] Indeed, the activity of the metal catalyst for these reactions is correlated to the nature of the metal.

3.2. Surface Adsorption of Key Intermediates. In our recent publication,[38] we thoroughly investigated ethanol-derived species during the ethanol decomposition course; thus, in this paper, we focus on some new $C_xH_yO_z$ (x = 1 or 2; y = 1−4, z = 1 or 2) species caused by the water involvement. Table 1 shows the optimal adsorption site, adsorption energy (E_{ad}), and some important geometric parameters. It can be seen that all studied species prefer the step-edge sites because of the

low coordination. The $C_xH_yO_z$ species interact with the Rh step edge through Rh−C or Rh−O or Rh−C−O−Rh oxymetalla-cycle, depending on the saturation of the molecule. All optimized structures are displayed in the Supporting Information (Figure S1), and our results are in good agreement with previous literature data.[55]

According to experimental reports, acetaldehyde (CH_3CHO) is one of the key intermediates in the low-temperature ethanol steam reforming reaction.[5] We first investigated the adsorption of CH_3CHO on various possible adsorption sites on the Rh(211) surface. It was found that the acetaldehyde molecule interacts with the Rh step edge via both an α-C and O (C_α-Rh = 2.093 Å, O−Rh = 2.057 Å). As shown in Supporting Information Figure S1, the C−O bond is almost parallel to the step edge, and the bond length is slightly stretched to 1.297 Å, as compared with 1.219 Å in the gas CH_3CHO molecule. This adsorption leads to an E_{ad} of −1.09 eV, which is very close to the value (−1.12 eV) reported in the previous literature.[55]

Because of the water involvement, extra OH groups are introduced into the system, which can possibly result in some new alcohol and carboxylic acid species, such as CH_xOH (x = 1−3) and CH_xCOOH (x = 2 or 3). We studied the adsorption of these species as well as the corresponding coadsorption systems. For example, for CH_3OH, CH_2OH, and CHOH, the most favorable adsorption site moves from the edge top site to the edge bridge site, and the adsorption energies in increasing order are the following: CH_3OH (−0.58 eV) < CH_2OH (−2.35 eV) < CHOH (−3.82 eV). Compared with alcohol, the carboxylic acid is more complicated because there is one more adsorption active site for the carbonyl group in addition to the hydroxyl group. On the basis of our calculations, we found that
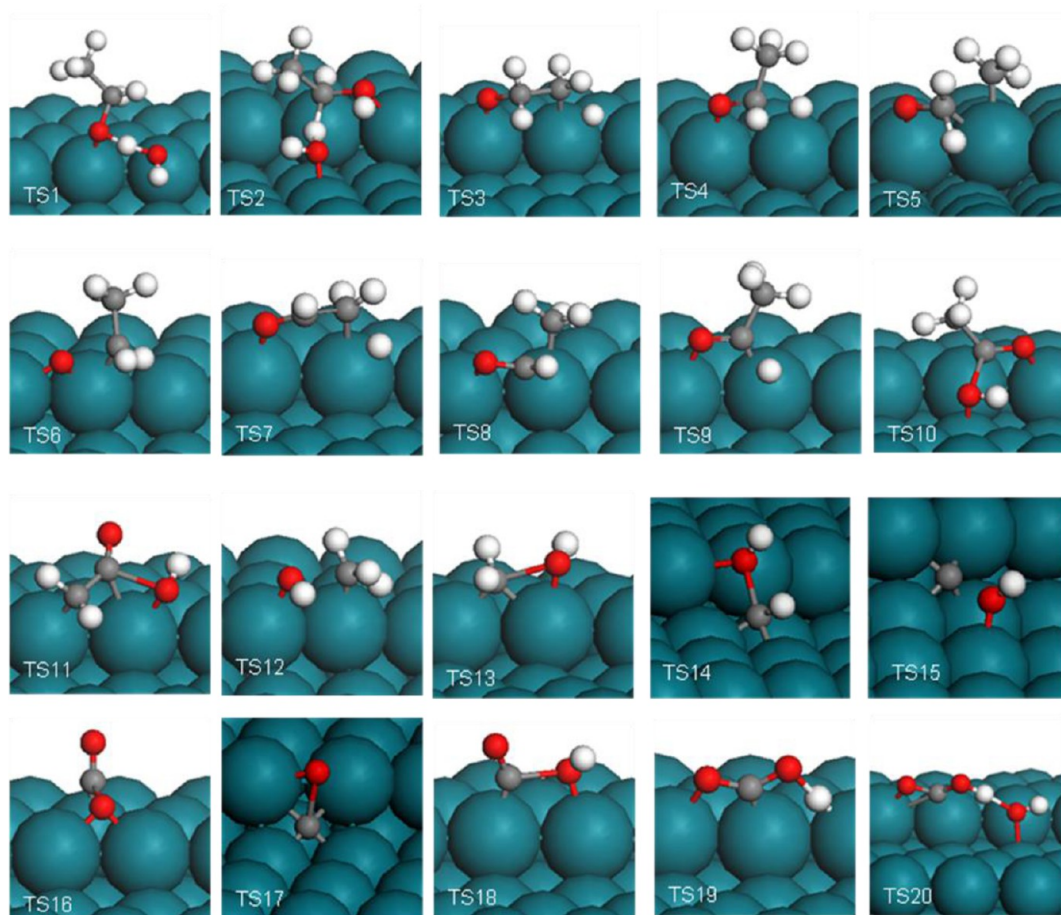
Figure 4. Configurations of transition states involved in Figure 3.

carboxylic acid species favor formation of an oxymetallacycle at the Rh step edge.

In the case of CH_3COOH, we considered two adsorption modes: (1) The O−C−O adsorption mode: CH_3COOH interacts with the surface step edge Rh via a hydroxyl oxygen (close to the top site with O−Rh = 2.286 Å) and carbonyl carbon and oxygen (coadsorbed on an edge Rh atom; O−Rh = 2.124 Å and C−Rh = 2.185 Å, respectively). The $C−O_{hydroxyl}$ bond is stretched to 1.447 Å from the 1.366 Å in CH_3COOH gas phase, and the binding leads to an adsorption energy of −0.57 eV. (2) The carbonyl C−O adsorption mode: the molecule adsorbs onto the step edge with O sitting at the edge bridge site (O−Rh = 2.215 and 2.206 Å), and C is at an off-edge top site with C−Rh = 2.338 Å. In fact, the adsorption energy caused by the second adsorption mode is −0.62 eV, which is slightly more stable than the O−C−O binding mode. Relative to saturated CH_3COOH, the unsaturated CH_2COOH is found to have a stronger adsorption energy on the Rh (211) surface (−2.32 eV). CH_2COOH binds to the step edge in a stable bidentate configuration via both an unsaturated C atom and a hydroxyl O atom (see Supporting Information Figure S1).

In addition, comparing the two isomers of COOH, it was found that the adsorption energy of *trans*-COOH on the Rh(211) surface is very close to that of *cis*-COOH. The *trans*-COOH (or *cis*-COOH) sits on the step edge with carbonyl C−Rh = 1.982 Å (1.979 Å for *cis*) and carbonyl O−Rh = 2.139 Å (2.144 Å for *cis*) (see Supporting Information Figure S1), respectively, leading to the adsorption energy of −2.91 eV

(−2.95 eV for *cis*). The similar adsorption behavior can also be observed on Pt (111) surface, on which *trans*-COOH is 0.05 eV higher than *cis*-COOH.[56]

3.3. Water Effect on the Ethanol Decomposition. Water is a critical reactant in the ethanol steam reforming process and, to a large degree, controls the real reaction mechanism. In our recent publication,[38] we systematically investigated ethanol decomposition on the Rh(211) surface and found C_α−H is the most likely reaction pathway, with the lowest energy barrier of 0.66 eV, followed by the O−H path, with the second lowest energy barrier of 0.88 eV. On the basis of those results, we further consider the influence of water participation (mainly the hydroxyl group) on the entire reaction course. In the beginning, various OH-involved coadsorption systems, including OH + CH_3CH_2OH, OH + CH_3CO, OH + CH_2CO, OH + CH_x ($x = 0, 1, 2, 3$) and OH + CO, were examined. We found that the OH group is always located at the bridge site on the Rh step edge, and the coadsorption energy ranges from −4.23 to −11.64 eV. The details about adsorption energies are summarized in Supporting Information Table S1. Considering the water involvement, the whole reaction can be divided into two parts: the first part is the ethanol decomposition with the aid of water, and the second part is the water-gas shift reaction.

In terms of our previous theoretical work,[38] we selected C_α−H and O−H path as the starting point to investigate the ethanol decomposition in the presence of water. As shown in Figure 3, the barrier of the O−H path is significantly reduced from 0.88 to 0.32 eV in the presence of the hydroxyl group,

whereas the barrier of the C_α−H path increases to 1.72 eV (compared with 0.66 eV without the help of OH group). At the transition state of the O−H pathway (TS1), the OH in H_2O interacts with the OH in CH_3CH_2OH by a H bond. As shown in Figure 4 (TS1), a near-to-linear $O_{(CH_3CH_2OH)}$−H−$O_{(H_2O)}$ is formed, with $O_{(CH_3CH_2OH)}$−H equal to 1.250 Å, H−$O_{(H_2O)}$ equal to 1.182 Å, and $O_{(CH_3CH_2OH)}$−$O_{(H_2O)}$ distance being 2.400 Å, which is close to the O−H⋯O hydrogen bond length of 2.73 Å.[57] It can be seen that the H-bonding effect greatly stabilizes the TS1 configuration, and thus, it lowers the energy barrier of hydroxyl dehydrogenation. This situation can also be observed in CO oxidation and dehydrogenation reactions with the help of water.[56] In the case of the C−H path, compared with transfer to a nearby OH group (E_a = 1.72 eV, TS2), an α-H in ethanol is more easily transferred to the Rh surface (E_a = 0.66 eV in the absence of an OH group). It should be noted that the initial bond-breaking order in ethanol is reversed because of the participation of water; that is, the O−H path to produce ethoxy (CH_3CH_2O) is more facile than the C−H path. Thus, a totally different reaction mechanism for the ethanol steam reforming reactions is expected in this work.

For the further degradation of ethoxy (CH_3CH_2O), there are four possible reaction pathways to be considered, including C_α−H, C_β−H, C−C, and C−O bond cleavage. As shown in Figure 3, C−C and C−O bond scission are the most difficult reaction pathways, with identical high-energy barriers of 1.55 eV. Compared with dissociation, the H removal at this step is easier because of the relatively low energy barrier of <1 eV. It can be seen that α-H elimination to produce acetaldehyde is the most favorable reaction pathway with the lowest energy barrier of 0.69 eV, which is 0.28 eV lower than that of β-H removal. At the transition state of the C_α−H path (TS4), the C_α−H bond breaks over a Rh atom at the step edge with a C−H distance of 1.605 Å. The C−O bond is slightly reduced (1.339 Å, between 1.355 Å in gas phase CH_3CH_2O and 1.219 Å in gas phase CH_3CHO) and tilted to the Rh step with O−H and C_α−H distances of 1.999 and 2.353 Å, respectively. Our calculations indicate that acetaldehyde (CH_3CHO) is an important intermediate in the presence of water, although it is excluded in the dry ethanol decomposition process on either the Rh(111) or Rh(211) surface. This result is consistent with our experimental observations and further provides qualitative confirmation of the structure of the observed C_2H_4O species (see Figure 1).

The yielding acetaldehyde is easily degraded because both C−C and C−H bond-breaking have an energy barrier below 1 eV. Among the three possible bond scissions, C_α−H bond-breaking has the lowest energy barrier (0.19 eV) compared with C−C (0.89 eV) and C_β−H bond-breaking (0.69 eV). These findings explain our previous experimental results and answer why acetyl (CH_3CO) can be observed in DRIFTS studies.[23] In addition, the sequential α-dehydrogenations (TS4 and TS9) from the acetaldehyde have very similar transition state configurations (see Figure 4), where the C−O bond binds to the Rh step edge in a bidentate configuration. At the TS9, the dissociating C_α−H distance is 1.464 Å, and the C−O double bond is almost parallel to the Rh step edge, with C_α−Rh and O−Rh distances of 2.027 and 2.109 Å, which are close to the final state (i.e., optimal adsorption mode of CH_3CO with $d_{\alpha-C-Rh}$ = 1.949 Å and d_{O-Rh} = 2.121 Å).[38]

For the CH_3CO intermediate, there are two possibilities: (1) further degradation and (2) reacting with a hydroxyl group to produce acetic acid (CH_3COOH). Our previous studies on CH_3CO dissociation on the Rh(211) surface indicated that the route via CH_2CO is ruled out, and the reaction proceeds via methyl elimination, where the C−C bond-breaking is the most difficult step because of its relatively high energy barrier of 0.92 eV (see Figure 3).[38] Actually, the decarbonylation or dehydrogenation of the CH_3CO species largely depends on the identity of the metal. It was reported that a Pt(211) surface has preference to form ketene (CH_2CO) rather than a methyl group in the degradation of acetyl species, which is different from a Rh(211) surface. In the case of association reactions, we found that the energy barrier to couple CH_3CO and OH is 1.09 eV starting from a [OH + CH_3CO] coadsorption state. Judging from the reaction barriers, we can see that acetic acid formation is more difficult than acetyl decarbonylation (E_a = 0.92 eV); thus, the CH_3CO + OH association to produce acetic acid is not favored at this step.

Because of the presence of water, we further considered possible reactions between the hydroxyl group and chemical species (such as CH_x; x = 0−3) produced in the course of acetyl decomposition. We found that the OH addition has a sizable energy barrier, ranging from 1.26 eV (TS13 for CH_2 + OH) to 1.80 eV (TS15 for C + OH), 1.59 eV at TS12 for CH_3 + OH coupling, and 1.60 eV of TS14 for CHOH formation in between. Obviously, the reaction barrier of the association process is much higher than that in the corresponding dissociation process; that is, the activation energy is 0.23 eV, 0.38, and 0.70 eV for the H abstraction from CH_3, CH_2, and CH, respectively. Thus, the OH addition channels to produce alcohol (CH_xOH) are ruled out. It seems that CO and C residues are the most likely ethanol dissociation products on the Rh(211) surface in an aqueous environment.

As shown in Figure 5, the energy profile of ethanol decomposition on Rh(211) with the aid of water has been
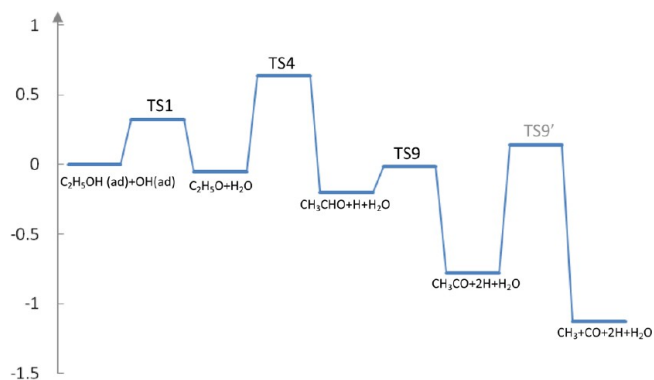

Figure 5. The potential energy diagram of ethanol decomposition to a methyl group on Rh(211) with the aid of water.

built in this work. The total energy of the initial ethanol−OH coadsorption state is set to 0, and all other energies, including energies for transition states, intermediate states, and final states, refer to this value. If we compare the reaction pathways of ethanol decomposition with and without[38] the aid of water, we can see that the acetyl (CH_3CO) is an important dividing point. Before the acetyl, the reaction intermediates are different in the two scenarios; however, after that, the reactions walk along the same route. Thus, only the energy profile of the ethanol decomposition to [CH_3 + CO] is plotted in Figure 5. For the profile of the energy change in the sequential

dehydrogenation of the CH_3 group, it has been calculated in reference 38. As shown in Figure 5, the reaction starts with the hydroxyl dehydrogenation to produce CH_3CH_2O, followed by the sequential α-H elimination, yielding CH_3CO. It can be seen that producing CH_3CO via CH_3CHO is a typical exothermic reaction, with a reaction energy of 0.58 eV, whereas the prior dehydrogenation reactions, regardless of breaking the O−H bond in CH_3CH_2OH ($\Delta E = 0.05$ eV) or breaking the C_α−H bond of CH_3CH_2O ($\Delta E = 0.15$ eV) are almost thermoneutral. Judging from the energy barriers, the reaction is slowed down by the C−C bond-breaking in CH_3CO, which has a higher energy barrier (0.92 eV) than the previous progressive H elimination (up to 0.69 eV) and the following stepwise methyl dehydrogenation (E_a up to 0.70 eV).

Because of the presence of water, the reaction will not end with a single C species; the generated C and CO could be further oxidized by O or OH group. We found that C oxidation reactions occur at the Rh step with relatively high activation energies: 1.63 eV for C + O → CO and 1.80 eV for C + OH → COH. It is further verified that C accumulation is a major problem, resulting in the Rh catalyst's deactivation.[5] In fact, catalyst deactivation caused by the deposition of carbonaceous species is a common issue for various transition metal surfaces. It was reported that the Pt{111} and Pt{211} surfaces also suffer from poisoning of stable intermediates in ethanol oxidation.[58] Experimental evidence has shown that the amount of C formation is correlated to the reaction conditions.[24,59] Recently, Mattos and co-workers reviewed catalyst deactivation during ESR and stated that the increase in the reaction temperature and H_2O-to-ethanol molar ratio favors a decrease in carbon deposition.[5]

Compared with C residue, it seems that CO oxidation reactions are more facile as a result of relatively lower barriers. Starting from CO, two channels are considered including oxidized by O atom and OH group. We found that OC−O coupling has an energy barrier of 1.10 eV (TS16) with a OC−O distance of 1.812 Å, which is about 0.3 eV higher than those on the Pt (111) (0.80 eV)[56] and Pd (111) surfaces (0.87 eV).[60] Compared with the CO + O association (1.10 eV), CO oxidation by the OH group has a higher energy barrier of 1.31 eV; however, if we measure the energy difference between the deeply lying intermediate [CO + OH + H] and TS16 [CO···O + 2H] (see Figure 6a), we can see that the barrier of the CO_2 formation is increased to 1.23 eV, which is slightly lower than that of CO + OH coupling by 0.08 eV. Thus, CO oxidation by O and the OH group are two competing channels.

Gong and Hu investigated the reaction of CO + OH → COOH → CO_2 + H on thePt(111) surface and found that COOH formation (0.44 eV) occurs easily compared with CO_2 formation (1.02 eV); however, on the basis of our calculations, on the Rh (211) surface, COOH dehydrogenation to form CO_2 has a lower energy barrier than CO + OH coupling to produce COOH ($E_a = 1.31$ eV). As shown in Figure 6a (blue path), in the absence of an extra OH group, the whole process is an endothermal process with a ΔE of 0.64 eV. From association (CO + OH) to dissociation (CO_2 + H), the energy barrier decreases from 1.31 eV (1.30 eV with ZPE correction) to 0.90 eV (0.78 eV with ZPE correction). Meanwhile, the effective energy barrier required for converting CO to CO_2 via an OH group is as high as 1.63 eV; however, the case is different when the influence of an extra OH group was considered in this process. In Figure 6b, it can be seen that H bonding in this system significantly facilitates CO_2 formation. There is almost
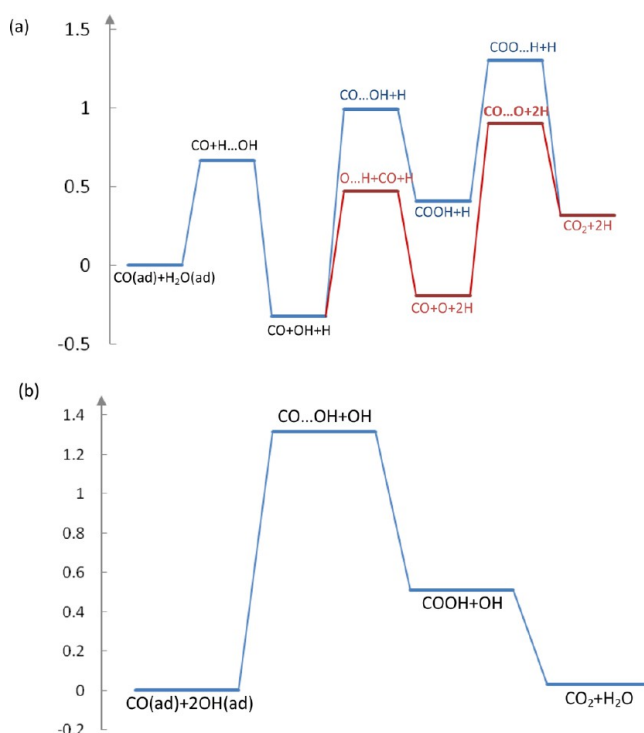

Figure 6. Profile of the energy change (a) in the CO oxidation reactions (CO + H_2O → COOH + H → CO_2 + 2H (blue); CO + H_2O → CO + O + 2H → CO_2 + 2H (red)) and (b) in CO oxidation with an extra OH group (CO + 2OH → COOH + OH → CO_2 + H_2O).

no energy barrier for COO−H bond-breaking in the presence of the second OH group. In this case, the entire reaction is almost a thermoneutral process with a ΔE of 0.03 eV, and the reaction is controlled by the CO + OH association step. In addition, we noticed that the sizable activation barrier of converting CO can also account for the high selectivity of CO and the low selectivity of CO_2 at 300 °C, whereas the order is reversed when the temperature is enhanced to 500 °C (see Figure 1).

Comparing the ethanol decomposition process (highest barrier of 0.92 eV for C−C bond cleavage in CH_3CO; see Figure 3) and the water-gas shift reactions (highest barrier of 1.31 eV for CO−OH coupling; TS18 in Figure 3), it seems that the bottleneck of the whole steam reforming process on stepped Rh (211) is the water-gas shift reaction, that is, CO + H_2O → CO_2 + H_2. Thus, to further improve catalytic performance of Rh catalyst and enhance the yield of H_2, one plausible way is to facilitate the water−gas shift reaction by introducing a second metal catalyst, such as Fe, Pt, Cu, or Au into the rhodium matrix.

Recently, Chen and co-workers successfully developed a rhodium−iron catalyst to help increase the yield of hydrogen gas in the ethanol steam reforming. Iron oxide is a standard industrial catalyst component used in the water-gas shift process. The experimental findings revealed that the addition of iron oxide remarkably enhances hydrogen output to about 4 units of hydrogen gas from every ethanol molecule, without the CO byproduct.[25]

In addition, other good candidates were also explored by some research groups. Cu is a classical catalyst for the low-temperature water-gas shift reaction. It has been reported that the reaction barrier for the CO(ads)−OH(ads) coupling

reaction is as low as 0.35, 0.33, and 0.60 eV on Cu(111), Cu(100), and the Cu_{29} cluster, respectively.[61−63] In addition, the recent theoretical studies on a Au_{38} cluster revealed that the energy barrier is further reduced to 1.15 kcal/mol (0.05 eV),[64] which is at least 0.3 eV lower than that on a Cu catalyst. However, we noticed that the activation energies of the $H_2O \rightarrow$ H + OH dissociation reaction on both Au and Cu catalyst are sizable, that is, 1.36 eV (31.41 kcal/mol) on Au_{38},[64] 1.36 eV on Cu(111),[61] 1.13 eV on Cu(100),[62,63] 0.93 eV on Cu_{29} cluster,[62,63] compared with that on a Rh(211) surface (0.66 eV). Therefore, the addition of the second metal catalyst promoting the water-gas shift reaction would combine the advantages of both components and, thus, enhance the catalytic performance for ethanol steam reforming reactions.

4. CONCLUSION

We have combined DFT calculations with experiments to study the ethanol steam reforming reaction on a Rh catalyst. The results indicate that water is an important reactant that significantly affects the ethanol decomposition on the Rh(211) surface. With the aid of water, the ethanol decomposition proceeds first via a hydroxyl dehydrogenation, followed by sequential α-dehydrogenation, and the generated acetyl (CH_3CO) undergoes direct C−C bond-breaking with a relatively high energy barrier of 0.92 eV. It was found that compared with coupling with a OH group to produce alcohol, the further degradation of CH_x ($x = 1−3$) is more facile. Regarding the residue C oxidation reaction, it has a sizable energy barrier of 1.63 eV, which confirmed that the C accumulation could cause Rh catalyst deactivation. In addition, the DFT calculations indicated that the water-gas shift reaction is paramount in the ethanol steam reforming process. Thus, one strategy to increase H_2 yield is to refine the catalyst to facilitate these related reactions. The detailed theoretical calculations plus experimental evidence in this work provide new insight into the working mechanism of the ethanol steam reforming reaction on Rh-based catalysts.

■ ASSOCIATED CONTENT

Ⓢ Supporting Information

Optimized configurations of important intermediates shown in Table 1; TS for H + H association; coadsorption energies of coadsorption systems on a Rh(211) surface; reaction energies for elementary steps; reaction barriers with and without zero-point energy correction (ΔZPE) for important elementary steps shown in Figures 2, 5, and 6. This information is available free of charge via the Internet at http://pubs.acs.org/.

■ AUTHOR INFORMATION

Corresponding Author

*E-mail: zhangj@ihpc.a-star.edu.sg.

Notes

The authors declare no competing financial interest.

■ REFERENCES

(1) Haryanto, A.; Fernando, S.; Murali, N.; Adhikari, S. *Energy Fuels* **2005**, *19*, 2098−2106.
(2) Anderson, J. R.; Boudart, M. *Catalysis, Science and Technology*; Springer: Berlin, 1984; Vol. 5, p 1.
(3) Palo, D. R.; Dagle, R. A.; Holladay, J. D. *Chem. Rev.* **2007**, *107* (10), 3992−4021.
(4) Ni, M.; Leung, D. Y. C.; Leung, M. K. H. *Int. J. Hydrogen Energy* **2007**, *32* (15), 3238−3247.
(5) Mattos, L. V.; Jacobs, G.; Davis, B. H.; Noronha, F. B. *Chem. Rev.* **2012**, *112* (7), 4094−4123.
(6) Cavallaro, S.; Chiodo, V.; Freni, S.; Mondello, N.; Frusteri, F. *Appl. Catal., A* **2003**, *249* (1), 119−128.
(7) Bilal, M.; Jackson, S. D. *Catal. Sci. Technol.* **2013**, *3* (3), 754−766.
(8) Jacobs, G.; Keogh, R. A.; Davis, B. H. *J. Catal.* **2007**, *245* (2), 326−337.
(9) Bilal, M.; Jackson, S. D. *Catal. Sci. Technol.* **2012**, *2* (10), 2043−2051.
(10) Carbajal Ramos, I. A.; Montini, T.; Lorenzut, B.; Troiani, H.; Gennari, F. C.; Graziani, M.; Fornasiero, P. *Catal. Today* **2012**, *180* (1), 96−104.
(11) Zhang, B.; Cai, W.; Li, Y.; Xu, Y.; Shen, W. *Int. J. Hydrogen Energy* **2008**, *33* (16), 4377−4386.
(12) Denis, A.; Grzegorczyk, W.; Gac, W.; Machocki, A. *Catal. Today* **2008**, *137* (2−4), 453−459.
(13) Fatsikostas, A. N.; Kondarides, D. I.; Verykios, X. E. *Catal. Today* **2002**, *75* (1−4), 145−155.
(14) Chiou, J. Y. Z.; Wang, W.-Y.; Yang, S.-Y.; Lai, C.-L.; Huang, H.-H.; Wang, C.-B. *Catal. Lett.* **2013**, *143* (5), 501−507.
(15) Lovon, A. S. P.; Lovon-Quintana, J. J.; Almerindo, G. I.; Valenca, G. P.; Bernardi, M. I. B.; Araujo, V. D.; Rodrigues, T. S.; Robles-Dutenhefner, P. A.; Fajardo, H. V. *J. Power Sources* **2012**, *216*, 281−289.
(16) Kugai, J.; Subramani, V.; Song, C. S.; Engelhard, M. H.; Chin, Y. H. *J. Catal.* **2006**, *238* (2), 430−440.
(17) Cobo, M.; Pieruccini, D.; Abello, R.; Ariza, L.; Fernando Cordoba, L.; Conesa, J. A. *Int. J. Hydrogen Energy* **2013**, *38* (14), 5580−5593.
(18) Aupretre, F.; Descorme, C.; Duprez, D.; Casanave, D.; Uzio, D. *J. Catal.* **2005**, *233* (2), 464−477.
(19) Roh, H. S.; Wang, Y.; King, D. L.; Platon, A.; Chin, Y. H. *Catal. Lett.* **2006**, *108* (1−2), 15−19.
(20) Kugai, J.; Velu, S.; Song, C. *Catal. Lett.* **2005**, *101*, 255−263.
(21) Frusteri, F.; Freni, S.; Spadaro, L.; Chiodo, V.; Bonura, G.; Donato, S.; Cavallaro, S. *Catal. Commun.* **2004**, *5* (10), 611−615.
(22) Diagne, C.; Idriss, H.; Kiennemann, A. *Catal. Commun.* **2002**, *3* (12), 565−571.
(23) Zhong, Z.; Ang, H.; Choong, C.; Chen, L.; Huang, L. *Phys. Chem. Chem. Phys.* **2009**, *11*, 872−880.
(24) Roh, H.-S.; Platon, A.; Wang, Y.; King, D. L. *Catal. Lett.* **2006**, *110* (1−2), 1−6.
(25) Chen, L.; Choong, C. K. S.; Zhong, Z.; Huang, L.; Ang, T. P.; Hong, L.; Lin, J. *J. Catal.* **2010**, *276* (2), 197−200.
(26) Graschinsky, C.; Laborde, M.; Amadeo, N.; Le Valant, A.; Bion, N.; Epron, F.; Duprez, D. *Ind. Eng. Chem. Res.* **2010**, *49* (24), 12383−12389.
(27) Goerke, O.; Pfeifer, P.; Schubert, K. *Appl. Catal., A* **2009**, *360* (2), 232−241.
(28) Campos-Skrobot, F. C.; Rizzo-Domingues, R. C. P.; Fernandes-Machado, N. R. C.; Cantao, M. P. *J. Power Sources* **2008**, *183* (2), 713−716.
(29) Can, F.; Le Valant, A.; Bion, N.; Epron, F.; Duprez, D. *J. Phys. Chem. C* **2008**, *112* (36), 14145−14153.
(30) Roh, H.-S.; Wang, Y.; King, D. L. *Top. Catal.* **2008**, *49* (1−2), 32−37.
(31) Virginie, M.; Araque, M.; Roger, A.-C.; Vargas, J. C.; Kiennemann, A. *Catal. Today* **2008**, *138* (1−2), 21−27.
(32) Mas, V.; Kipreos, R.; Amadeo, N.; Laborde, M. *Int. J. Hydrogen Energy* **2006**, *31*, 21−28.
(33) Choi, Y.; Liu, P. *Catal. Today* **2011**, *165*, 64−70.
(34) Li, M.; Guo, W.; Jiang, R.; Zhao, L.; Lu, X.; Zhu, H.; Fu, D.; Shan, H. *J. Phys. Chem. C* **2010**, *114*, 21493.
(35) Wang, J.-H.; Lee, C. S.; Lin, M. C. *J. Phys. Chem. C* **2009**, *113*, 6681−6688.
(36) Ma, Y.; Hernández, L.; Guadarrama-Pèrez, C.; Balbuena, P. B. *J. Phys. Chem. A* **2012**, *116*, 1409−1416.
(37) Syu, C.-Y.; Wang, J.-H. *ChemCatChem* **2013**, *5* (10), 3164−3174.

(38) Zhang, J.; Cao, X.-M.; Hu, P.; Zhong, Z.; Borgna, A.; Wu, P. *J. Phys. Chem. C* **2011**, *115*, 22429−22437.

(39) Gontard, L. C.; Chang, L.-Y.; Hetherington, C. J. D.; Kirkland, A. I.; Ozkaya, D.; Dunin-Borkowski, R. E. *Angew. Chem.* **2007**, *119*, 3757−3759.

(40) Behrens, M.; Studt, F.; Kasatkin, I.; Kühl, S.; Hävecker, M.; Abild-Pedersen, F.; Zander, S.; Girgsdies, F.; Kurr, P.; Kniep, B.-L.; Tovar, M.; Fischer, R. W.; Nørskov, J. K.; Schlögl, R. *Science* **2012**, *336*, 893−897.

(41) Kresse, G.; Hafner, J. *Phys. Rev. B* **1993**, *48*, 13115.

(42) Kresse, G.; Hafner, J. *Phys. Rev. B* **1994**, *49*, 14251.

(43) Bloechl, P. E. *Phys. Rev. B* **1994**, *50*, 17953.

(44) Kresse, G.; Joubert, D. *Phys. Rev. B* **1999**, *59*, 1758.

(45) Perdew, J. P.; Wang, Y. *Phys. Rev. B* **1992**, *45*, 13244.

(46) Lide, D. R., *CRC Handbook of Chemistry and Physics*. 76th ed.; CRC Press: New York, 1996.

(47) Choi, Y. M.; Liu, P. *J. Am. Chem. Soc.* **2009**, *131*, 13054.

(48) Alavi, A.; Hu, P.; Deutsch, T.; Silvestrelli, P. L.; Hutterm, J. *Phys. Rev. Lett.* **1998**, *80*, 3650.

(49) van Grootel, P. W.; Hensen, E. J. M.; van Santen, R. A. *Surf. Sci.* **2009**, *603*, 3275−3281.

(50) Pozzo, M.; Carlini, G.; Rosei, R.; Alfè, D. *J. Chem. Phys.* **2007**, *126*, 164706.

(51) Wilke, S.; Natoli, V.; Cohen, H. *J. Chem. Phys.* **2000**, *112*, 9986.

(52) Meng, S.; Wang, E. G.; Gao, S. *Phys. Rev. B* **2004**, *69*, 195404.

(53) Michaelides, A.; Ranea, V. A.; de Andres, P. L.; King, D. A. *Phys. Rev. Lett.* **2003**, *90*, 216102.

(54) Tang, Q.-L.; Liu, Z.-P. *J. Phys. Chem. C* **2010**, *114*, 8423−8430.

(55) Kapur, N.; Hyun, J.; Shan, B.; Nicholas, J. B.; Cho, K. *J. Phys. Chem. C* **2010**, *114*, 10171.

(56) Gong, X.-Q.; Hu, P. *J. Chem. Phys.* **2003**, *119*, 6324.

(57) Brown, I. D. *Acta Crystallogr.* **1976**, *A32*, 24.

(58) Wang, H.-F.; Liu, Z.-P. *J. Am. Chem. Soc.* **2008**, *130* (33), 10996−11004.

(59) Platon, A.; Roh, H.-S.; King, D. L.; Wang, Y. *Top. Catal.* **2007**, *46*, 374−379.

(60) Zhang, J.; Jin, H.; Sullivan, M. B.; Lim, F. C. H.; Wu, P. *Phys. Chem. Chem. Phys.* **2009**, *11*, 1441−1446.

(61) Gokhale, A. A.; Dumesic, J. A.; Mavrikakis, M. *J. Am. Chem. Soc.* **2008**, *130* (4), 1402−1414.

(62) Liu, P.; Rodriguez, J. A. *J. Chem. Phys.* **2007**, *126* (16), 164705.

(63) Rodriguez, J. A.; Liu, P.; Hrbek, J.; Evans, J.; Perez, M. *Angew. Chem., Int. Ed.* **2007**, *46* (8), 1329−1332.

(64) Lin, R.-J.; Chen, H.-L.; Ju, S.-P.; Li, F.-Y.; Chen, H.-T. *J. Phys. Chem. C* **2012**, *116*, 336.